EARTHQUAKE ENGINEERING AND STRUCTURAL DYNAMICS
*Earthquake Engng Struct. Dyn.* 2003; **32**:1867–1896 (DOI: 10.1002/eqe.306)

# Multi-variable relations for soil effects on seismic ground motion

George D. Bouckovalas*,† and Achilleas G. Papadimitriou

*Geotechnical Department, Faculty of Civil Engineering, National Technical University of Athens, Greece*

## SUMMARY

Soil effects on peak ground acceleration, velocity and elastic response spectra (5% damping) are expressed by simple approximate relations in terms of five key parameters: (a) the fundamental vibration period of the non-linear soil, $T_S$, (b) the period of a bedrock site of equal thickness, $T_b$, (c) the predominant excitation period, $T_e$, (d) the peak seismic acceleration at outcropping bedrock, $a^b_{\max}$, and (e) the number of significant excitation cycles, $n$. Furthermore, another relation is proposed for the estimation of $T_S$ in terms of the soil thickness $H$, the average shear wave velocity of the soil $\bar{V}_{S,o}$ and $a^b_{\max}$. The aforementioned parameters were first identified through a simplified analytical simulation of the site excitation. The multivariable approximate relations were then formulated via a statistical analysis of relevant data from more than 700 one-dimensional equivalent-linear seismic ground response analyses, for actual seismic excitations and natural soil conditions. Use of these relations to back-calculate the numerical results in the database gives an estimate of their error margin, which is found to be relatively small and unbiased. The proposed relations are also independently verified through a detailed comparison with strong motion recordings from seven well-documented case studies: (a) two sites in the San Fernando valley during the Northridge earthquake, and (b) five different seismic events recorded at the SMART-1 accelerometer array in Taiwan. It is deduced that the accuracy of the relations is comparable to that of the equivalent-linear method. Hence, they can be readily used as a quick alternative for routine applications, as well as for spreadsheet computations (e.g. GIS-aided seismic microzonation studies) where numerical methods are cumbersome to implement. Copyright © 2003 John Wiley & Sons, Ltd.

KEY WORDS: earthquake; seismic motion; site effects; response spectra; seismic microzonation; GIS applications

## INTRODUCTION

Soil alters the characteristics of seismic waves in a way that the amplitude and the frequency content of seismic motions on the free soil surface differ from those on the surface of the

* Correspondence to: George D. Bouckovalas, 1 Iktinou Str., 151 26, Athens, Greece.
† E-mail: g.bouck@civil.ntua.gr

Contract/grant sponsor: The Earthquake Protection and Planning Organization of Greece

*Received 16 May 2002*
*Revised 22 November 2002*
*Accepted 24 January 2003*

outcropping bedrock. This phenomenon is widely known as 'soil amplification': a rather unfortunate choice of terminology because the term 'amplification' refers only to the amplitude and not the frequency content, and also because the soil may either amplify or de-amplify the seismic motion depending on various parameters studied in this paper. Nevertheless, the term is retained in this paper, simply for reasons of consistency with the relevant literature. Despite the fact that the topography of the ground and that of the bedrock basin are sometimes equally influential in altering the seismic ground motion and determining the overall site response, soil (amplification) effects are the primary geotechnical concern in the seismic design of civil engineering works.

In broad terms, the methods of estimating soil effects for design purposes may be divided into two categories.

(a) Empirical, which correlate seismic motion characteristics from actual recordings to soil conditions at the recording site, by means of a single soil parameter (e.g. References [1–8]).
(b) Numerical, which employ wave propagation theory either in the frequency or in the time domain and may simulate the details of any given soil profile and seismic excitation (e.g. SHAKE [9], SHAKE91 [10–12]).

The currently available single soil parameter empirical methods offer the advantage of immediate and fairly inexpensive application, but often fail to capture basic engineering aspects of soil-to-excitation interaction, such as resonance or phase difference effects [13]. On the other hand, numerical methods are site specific and capable of simulating most aspects of seismic soil response. Still, they have shortcomings since their application is often limited by the time and cost required in order to collect all necessary input data and to perform the analyses.

To fill this gap, a set of approximate multivariable relations is established herein, based on data from over 700 numerical ground response analyses, which were performed to simulate actual seismic excitations and natural soil conditions. This number of analyses may not be too large *per se*, but it did enable all parameters to vary within a wide range, making a regression analysis of the data reliable. Moreover, and to their benefit, these analyses were not 'blind' parametric runs, but were performed for actual design projects with significant input of engineering judgement.

To guide the input data selection and the regression analysis, the basic parameters of the relations were first identified by means of a closed-form analytical solution for uniform soil and harmonic base excitation. Furthermore, to verify their accuracy and robustness for practical applications, an extensive evaluation was performed against strong motion recordings from seven well-documented case studies, namely: (a) two sites in the San Fernando valley during the Northridge earthquake (17 January 1994), and (b) five seismic events in the SMART-1 accelerometer array in Taiwan.

With the proposed relations, approximate predictions of soil effects become more refined and suitable for engineering applications where detailed site-specific analyses are not justified or cannot be implemented (e.g. GIS-aided seismic microzonation studies). A similar compilation of actual seismological data, although unquestionably more rigorous, is presently not easy to perform, since only a relatively small part of the available recordings is adequately documented with regard to the engineering characteristics of the site and the seismic excitation.

 

## PARAMETER IDENTIFICATION

The basic parameters contributing to soil effects may be identified with the aid of wave propagation theory for a uniform, visco-elastic soil and bedrock profile under harmonic base excitation (e.g. Reference [14]). Thus, it can be shown that the ratio of the amplitude of motion at the free ground surface to the amplitude of motion at the outcropping bedrock is expressed as:

$$|A_s| = \frac{\exp\left[\xi_b \frac{T_b}{T_s}\left(\frac{\pi}{2}\frac{T_s}{T_e}\right)\right]}{\left|\cos\left(\frac{\pi}{2}\frac{T_s^*}{T_e}\right) + i\alpha^* \sin\left(\frac{\pi}{2}\frac{T_s^*}{T_e}\right)\right|} \tag{1}$$

where $T_e$ denotes the excitation period, $T_S^* = T_S(1-i\xi_S)$, $\alpha = (\rho_s/\rho_b)(T_b/T_s)$ and $\alpha^* = \alpha(1+i\xi_s)/(1-i\xi_s)$.

In the above relations the mass density and critical damping ratio of the soil are denoted as $\rho_S$ and $\xi_S$, respectively, while $T_S$ denotes the fundamental vibration period of the soil. The corresponding properties for the bedrock are denoted as $\rho_b$ and $\xi_b$, while $T_b$ is the fundamental period of vibration of a layer of outcropping bedrock with the same thickness $H$ as the soil.

For small values of the impedance ratio $\alpha$ and the critical damping ratio $\xi_S$, Equation (1) may be approximately written as:

$$|A_s| = \frac{\exp\left[\xi_b \frac{T_b}{T_s}\left(\frac{\pi}{2}\frac{T_s}{T_e}\right)\right]}{\sqrt{\cos^2\left(\frac{\pi}{2}\frac{T_s}{T_e}\right) + \left[\xi_{e,s}\left(\frac{\pi}{2}\frac{T_s}{T_e}\right)\right]^2}} \tag{2}$$

where:

$$\xi_{e,s} = \xi_s + \frac{2}{\pi}\alpha\frac{T_e}{T_s} \tag{3}$$

The previous analytical relations refer to the steady state response of the soil profile. To take into account the transient phase of the response, the amplification ratio $A_S$ has to be related to the duration of the base excitation, or to the number of cycles $n$. Thus, $A_S$ can be considered as a function of five independent factors: $T_b/T_S$, $T_S/T_e$, $\rho_S/\rho_b$, $\xi_S$, $\xi_b$ and $n$. Furthermore, for non-linear soils, the peak acceleration of the seismic excitation $a^b_{\max}$ should be added to the above factors as it affects both the fundamental period of the non-linear soil, $T_S$, and its critical damping ratio, $\xi_S$.

In the present study, priority is given to the effect of four of these factors: $T_S/T_e$, $T_b/T_S$, $a^b_{\max}$ and $n$. The effect of the remaining factors is overlooked, since $\xi_b$ and $\rho_S/\rho_b$ show generally little variability in nature, while $\xi_S$ is primarily a function of earthquake-induced shear strains and, in turn, of $a^b_{\max}$ and $n$.

## DATABASE AND STATISTICAL ANALYSIS

The proposed relations are based on a multivariable regression analysis of the input data and the results of over 700 numerical analyses of seismic ground response. The site model

 

used for these analyses consists of a number of horizontal soil layers, with non-linear visco-elastic response, resting upon uniform, linear visco-elastic bedrock. Computations follow the equivalent-linear method [9, 10], assuming vertical propagation of earthquake-induced shear waves from the seismic bedrock to the ground surface and vice versa.

The seismic excitations in the numerical analyses were applied at the surface of the outcropping seismic bedrock. In the majority of the analyses, the seismic bedrock was defined within Neogene or older geological formations, with small strain shear wave velocity $V_b = 550$ m/s and mass density $\rho = 2.2$ Mg/m$^3$. Nevertheless, cases of softer and stiffer bedrock formations were also examined.

The seismic excitations used for the analyses were actual strong motion recordings. Their predominant period, $T_e$, estimated as the period of the peak spectral acceleration, varies from 0.1 to 0.8 s, capturing a wide spectrum of potential earthquake events. Their duration is also highly variable, with the equivalent number of uniform cycles $n = 0.5$ to 24. Note that the value of $n$ for each excitation is estimated as the number of cycles in the time-history that exceed a level of acceleration equal to $a^b_{\max}(M-1)/10$, where $M$ is the earthquake magnitude. This empirical 'rule of thumb' is an extension of the relation between the equivalent uniform and the maximum shear strains adopted in the numerical analyses of seismic ground response [10].

The soil profiles used in the numerical analyses correspond to sites where geotechnical investigations were performed, including measurements (mainly crosshole) of shear wave velocity, as part of major infrastructure development projects in Greece (microzonation of urban centres or seismic design of tunnels, gas and oil transmission pipelines, etc). To increase further the range of site characteristics, analyses were also performed for a limited number of artificial soil profiles. Each artificial profile was obtained by uniform scaling (up or down) of the small strain shear wave velocity $V_{S,o}$ of all layers comprising the corresponding natural soil profile, without affecting layer thickness or any other characteristic. In all cases, the soil profiles considered in this study consist of alternating layers of sand, silt and gravel mixtures, as well as low plasticity clays and marls. Soil non-linearity in these analyses is introduced by shear modulus degradation and hysteretic damping increase curves. Lacking actual measurements, the experimental curves of Vucetic and Dobry [15] for soil materials with plasticity index $I_p$ between 0% and 50% were used for this purpose.

The overall variability of the site conditions is outlined in Table I by means of the range and frequency distribution of the principal site characteristics. In addition, this table provides the range and frequency distribution of the main parameters that affect soil amplification, namely: $T_S/T_e$, $T_b/T_S$, $a^b_{\max}$ and $n$. Observe that site characteristics as well as soil amplification parameters cover a wide range of values, typical for the great majority of potential case studies in practice.

The equivalent-linear method has been the standard analysis tool worldwide for the last thirty years and its overall accuracy for low-to-moderate levels of ground shaking has been directly or indirectly demonstrated in a number of recent case studies, through comparison with data from seismic array recordings (e.g. References [16–20]). On the whole, the method is not to be used for unstable soils (e.g. liquefiable, very sensitive). When used for stable soils, criticism of the method has been mainly expressed for very deep soil sites and very strong excitation conditions, where the use of confining stress and frequency independent moduli and damping factors may lead to non-conservative low predictions of ground response [21, 22]. Conscious of the above limitations, compilation of the database of numerical analyses

 

Table I. Range and frequency distribution of parameters.

| Parameter | | Range | Frequency distribution |
|---|---|---|---|
| Soil thickness | $H$ (m) | 3.5–240 | 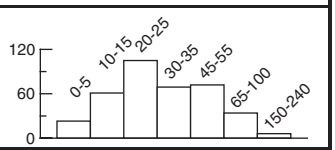  |
| Average small strain shear wave velocity of soil | $\overline{V}_{S,o}$ (m/s) | 50 −700 | 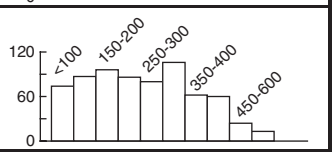  |
| Shear wave velocity in bedrock | $V_b$ (m/s) | 100 −1000 | 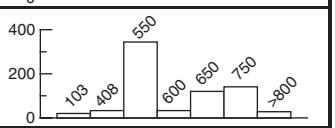  |
| Fundamental non-linear soil period | $T_S$ (s) | 0.04–3.33 | 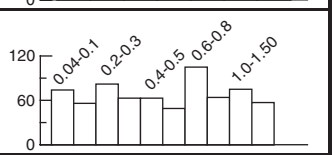  |
| Fundamental bedrock period | $T_b$ (s) | 0.02–1.75 | 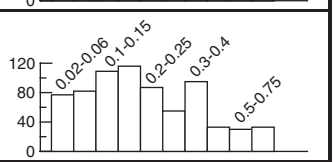  |
| Bedrock–to–soil impedance ratio | $T_b / T_S$ | 0.05– 0.95 | 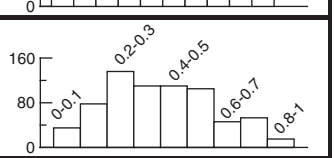  |
| Normalized soil period | $T_S / T_e$ | 0.06 −13.3 | 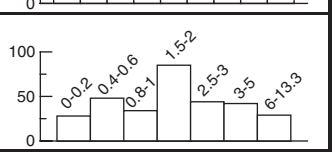  |
| Peak horizontal acceleration at outcropping bedrock | $a^b_{\max}$ $(g)$ | 0.01– 0.45 | 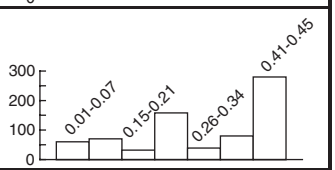  |
| Duration of seismic excitation | $n$ (cycles) | 0.5–24 | 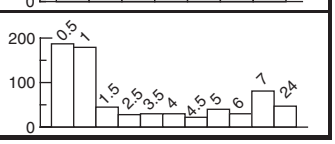  |

 

systematically avoided extreme site and excitation conditions. Namely, $a^b_{\max}$ never exceeded 0.45 $g$, while 85% of the sites are less than 55 m deep and have an average small strain shear wave velocity $\bar{V}_{s,o}$ higher than 120 m/s. For the remaining sites the equivalent linear predictions are less accurate, but they were retained in the database so that the full picture of the effect of the various parameters could be drawn.

The general form of the proposed relations was defined in advance of the statistical analysis of the relevant data, from a joint evaluation of appropriate analytical solutions (e.g. Equation (2)) and the trends exhibited by the numerical predictions themselves. The quantitative expression of the proposed relations was consequently established from a multivariable regression analysis of the entire database, according to the Newton–Raphson iterative procedure. Appropriate weights were used in connection with $a^b_{\max}$, an independent variable with significant influence and the least uniform statistical distribution (see Table I). The weights were inversely proportional to the percentile presence of the various $a^b_{\max}$ values in the database and aimed at counter-balancing the effect of having 39% of the cases performed for $0.41\,g \leqslant a^b_{\max} \leqslant 0.45\,g$.

To expedite the presentation of the results of the statistical analysis, the results of the equivalent-linear numerical simulations will hereafter be denoted as data, although they are also simulations and not actual data deduced from recordings.

## RELATIONS FOR PEAK SEISMIC MOTION PARAMETERS

### *Amplification of peak ground acceleration*

Figure 1 shows the variation of the relative amplification ratio for the peak ground acceleration, denoted hereafter as $A_a$, with the normalized soil period $T_S/T_e$. In this figure, the data are presented in pairs of groups, by maintaining two of the remaining free variables within a narrow range, and significantly changing the third variable.

Observe that the effect of normalized site period $T_S/T_e$ is similar in all figures. Namely, $A_a$ tends to 1.0 as $T_S/T_e$ tends to zero, it becomes maximum close to $T_S/T_e = 1.0$ and it decreases gradually as $T_S/T_e$ exceeds 1.0. This trend calls to mind the response of single-degree-of-freedom (SDOF or mass-spring-dashpot) systems subjected to harmonic base excitation. Hence, drawing upon the theory of SDOF vibrations under support excitation (e.g. Biggs [23], Chopra [24]) the data in Figure 1 have been fitted with the following general expression:

$$A_a = \frac{1 + C_{1,a}(T_s/T_e)^2}{\sqrt{[1 - (T_s/T_e)^2]^2 + C^2_{2,a}(T_s/T_e)^2}} \tag{4}$$

According to Equation (4), $A_a$ takes the following characteristic values:

$$A_a = \begin{cases} 1.0 & \text{for } T_s/T_e = 0 \\ (1 + C_{1,a})/C_{2,a} & \text{for } T_s/T_e = 1 \\ C_{1,a} & \text{for } T_s/T_e \to \infty \end{cases} \tag{5}$$

The fact that $A_a$ tends to a fixed, non-zero value at large normalized site periods ($T_S/T_e$) is the only basic difference from the response of a SDOF system, which eventually

 

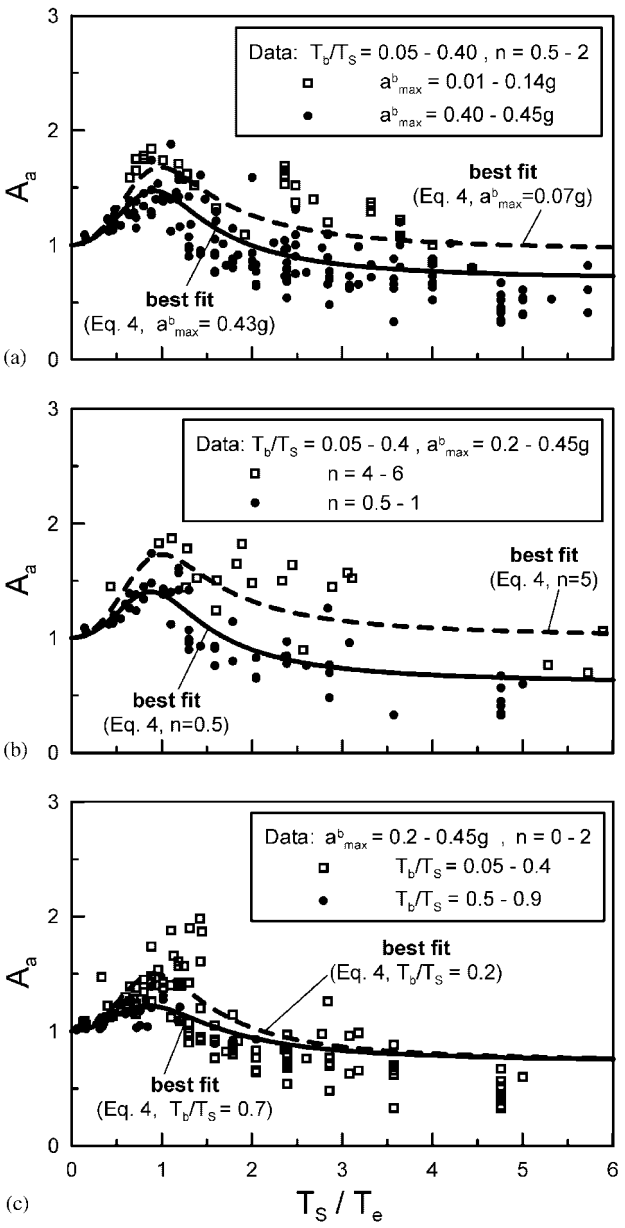


Figure 1. Effect of site and excitation parameters on $A_a$: (a) effect of peak ground acceleration $a^b_{\max}$; (b) effect of number of cycles $n$; (c) effect of soil-to-bedrock impedance ratio $T_b/T_S$.

diminishes to zero. This differentiation was conservatively introduced in order to take into account the contribution to the response of the higher modes of vibration of actual soil profiles.

 

In general, the coefficients $C_{1,a}$ and $C_{2,a}$ should be expressed as functions of the three remaining independent variables, i.e. $a^b_{\max}$, $T_b/T_S$ and $n$. However, the data in Figure 1 show that $C_{1,a}$ is not affected by $T_b/T_S$, but increases consistently as $n$ and $a^b_{\max}$ become higher and lower, respectively. Moreover, the value of $A_a$ at resonance increases with increasing $n$ and decreasing $a^b_{\max}$. Hence, it was assumed that $C_{1,a}$ can be expressed as a function of $a^b_{\max}$ and $n$ only:

$$C_{1,a} = d_{1,a}\left(\frac{a^b_{\max}}{g}\right)^{d_{2,a}} g(n) \tag{6}$$

with

$$g(n) = \frac{n^{d_{3,a}}}{1 + n^{d_{3,a}}} \tag{7}$$

and $d_{1,a} > 0$, $d_{2,a} < 0$, $d_{3,a} > 0$. Note that the general form of function $g$ provides an asymptotic increase of $C_{1,a}$ and $A_a$ towards the steady state values, at large number of cycles $n$. This effect resembles the transient response of SDOF systems at resonance conditions (e.g., Reference [24]), and is also consistent with the response displayed by the data in Figure 1(b).

Finally, the data in Figure 1(c) indicate that the peak value of $A_a$ tends rather to decrease as the normalized period of the bedrock $T_b/T_S$ becomes higher. This is reasonable since $T_b/T_S$ represents essentially the contrast in dynamic stiffness between the soil and the underlying bedrock, and it is consequently a measure of the radiation damping, i.e. the percentage of energy lost from seismic waves reflected back into the bedrock. To simulate this effect, $C_{2,a}$ was correlated to $T_b/T_S$ through a linear relation, of the same form as Equation (3), which describes the equivalent critical damping ratio for a uniform visco-elastic soil layer resting on flexible bedrock:

$$C_{2,a} = d_{4,a} + d_{5,a}\frac{T_b}{T_S} \tag{8}$$

with $d_{4,a}$ and $d_{5,a} > 0$.

The constants in Equations (6)–(8) were determined from a statistical analysis of all available data. This procedure led to a *best fit* relation for $d_{1,a} = 1.20$, $d_{2,a} = -0.17$, $d_{3,a} = 0.50$, $d_{4,a} = 1.05$ and $d_{5,a} = 0.57$. A conservative *upper bound* of the data was consequently taken by increasing $d_{1,a}$ to 1.75. This increase established that $A_a$ is over-predicted in 85% of the cases in the database.

Figure 2 presents a one-to-one comparison of $A_a$ values, based on the proposed relations and the equivalent-linear analyses for all the cases in the database. In addition, Figure 3 presents another comparison of the *best-fit* simulations and the data, in terms of the relative error $R_{A_a}$, defined as the difference between approximate predictions of $A_a$ and data normalized with respect to the latter. It is observed that the *best-fit* predictions for $A_a$ agree overall well with their numerical counterparts. In detail, the relative error has an overall standard deviation of about 24%, without any significant bias with regard to any of the factors entering Equation (5). The only exception concerns very flexible soil profiles ($T_S/T_e > 6$) over stiff bedrock ($T_b/T_S < 0.2$), undergoing relatively intense shaking ($a^b_{\max} > 0.40\,g$). The depicted conservatism applies to low values of $A_a$ ($< 0.60$) and is a product of the general form given to Equation (4). Specifically, this equation favors a better match near resonance (at $0.5 < T_S/T_e < 2.5$), where most detrimental effects of seismic motion are to be expected and where 50% of the data lie.

 

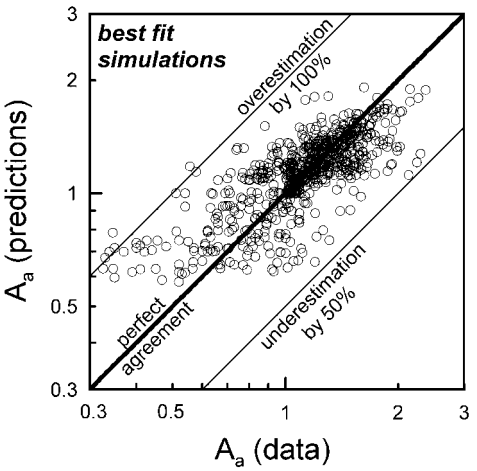


Figure 2. Summary comparison between predictions of $A_a$ from the approximate relations and their numerical estimates.

*Amplification of peak ground velocity*

Numerical predictions for the relative amplification of peak ground velocity ($A_V$) are plotted in Figure 4 against the normalized soil period $T_S/T_e$. Specifically, Figures 4(a)–(c) show examples of the effects of the bedrock-to-soil period ratio $T_b/T_S$, the peak bedrock acceleration $a^b_{\max}$ and the number of equivalent cycles $n$, respectively. The effect of the various factors on $A_V$ is similar to the case of $A_a$, except for two main differences. The first difference, shown in Figure 4(c), is that $A_V$ is not consistently affected by the duration of the seismic motion. The second difference, that becomes evident in all three parts of Figure 4, is that the maximum values of $A_V$ occur at normalized soil periods $T_S/T_e$ higher than one, i.e. beyond soil-to-excitation resonance. This is because the predominant period of the velocity time history for actual seismic motions is usually higher than that of the corresponding acceleration time history. For instance, this trend can be clearly observed in most tri-logarithmic representations of elastic response spectra, where the peak spectral velocity occurs at larger structural periods than the peak spectral acceleration.

According to the data in Figure 4, the maximum values of $A_V$ occur at approximately $T_S \cong 1.50T_e$. Hence, Equation (4) is re-written as:

$$A_V = \frac{1 + C_{1,V}(T_s/1.5T_e)^2}{\sqrt{[1-(T_s/1.5T_e)^2]^2 + C^2_{2,V}(T_s/1.5T_e)^2}} \tag{9}$$

where

$$C_{1,V} = d_{1,V}\left(\frac{a^b_{\max}}{g}\right)^{d_{2,V}} \tag{10}$$

$$C_{2,V} = d_{3,V} + d_{4,V}\,\frac{T_b}{T_s} \tag{11}$$

with $d_{2,V} < 0$, while $d_{3,V}$ and $d_{4,V} > 0$.

 

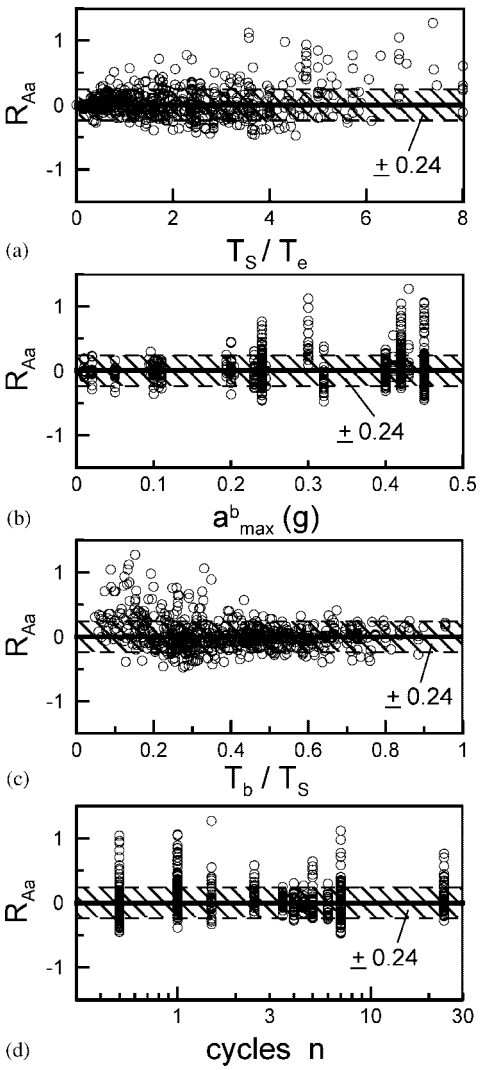


Figure 3. Evaluation of relative error in the computation of $A_a$ with the approximate relations (standard deviation of relative error = 0.24).

The constants in Equations (10) and (11) were again determined from a multi-variable regression analysis of all available data. According to this, the *best-fit* relation is obtained for $d_{1,V} = 0.88$, $d_{2,V} = -0.124$, $d_{3,V} = 1.087$ and $d_{4,V} = 0.598$, while increasing $d_{1,V}$ to 1.25 assures an overprediction for about 85% of the data (*upper bound* relation).

The *best-fit* predictions of $A_V$ are evaluated in Figures 5 and 6, in the same format as that used to evaluate $A_a$. The *best-fit* predictions of $A_V$ agree well with the data, as the overall standard deviation of the error is 20% without any consistent bias. The only exception concerns soil sites over relative stiff bedrock ($T_b/T_S < 0.2$), and undergoing intense shaking

 

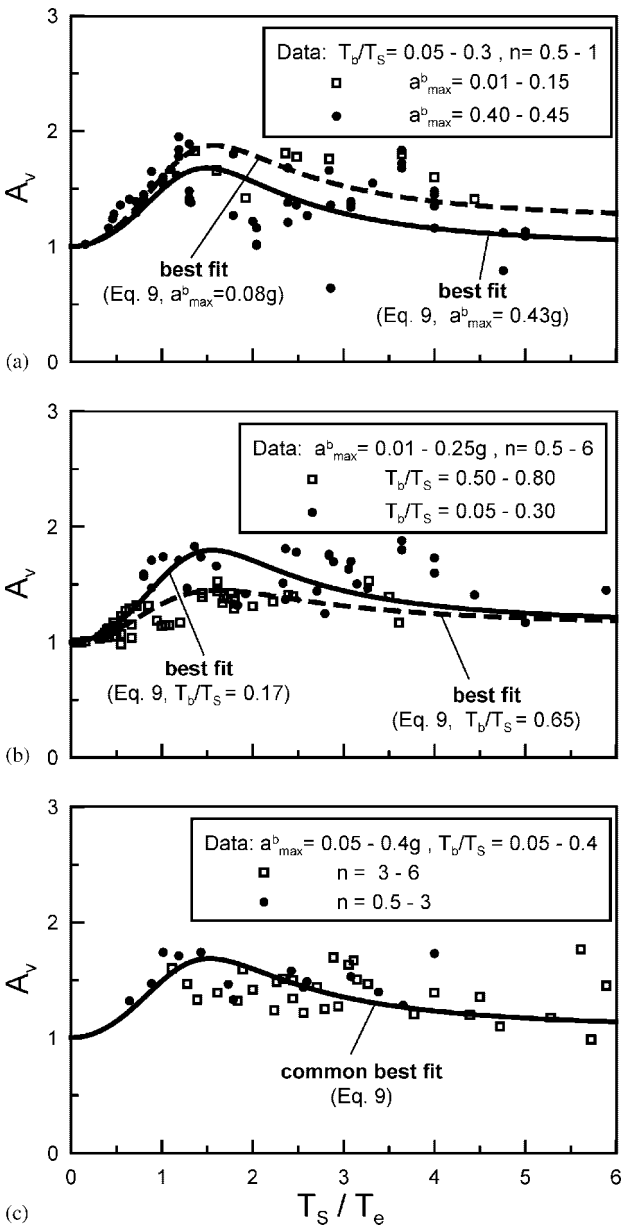


Figure 4. Effect of site and excitation parameters on $A_V$: (a) effect of peak ground acceleration $a^b_{\max}$; (b) effect of soil-to-bedrock impedance ratio $T_b/T_S$; (c) effect of number of cycles $n$.

($a^b_{\max} > 0.40\ g$) for which $A_V$ is overpredicted. Similarly to what is observed for $A_a$, this conservatism is a product of the form given to Equation (9) and applies to low $A_V$ values ($< 0.90$).

 

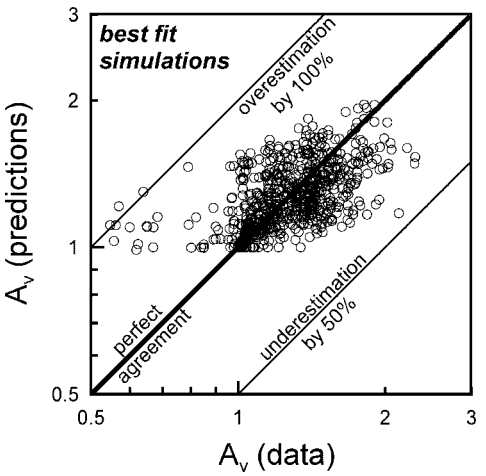


Figure 5. Summary comparison between predictions of $A_V$ from the approximate relations and their numerical estimates.

## RELATIONS FOR ELASTIC RESPONSE SPECTRA

To better study soil effects on the frequency content of the horizontal spectra, the emphasis is placed on the 5% damped normalized spectral acceleration $S_a^* = S_a/a_{\max}$ and the corresponding soil surface-to-bedrock outcrop amplification ratio:

$$A_{Sa}^* = \frac{(S_a^*)_{\text{soil}}}{(S_a^*)_{\text{bedrock}}} = \frac{S_a^s}{S_a^b}\,\frac{1}{A_a} \tag{12}$$

where $A_a$ is the amplification ratio for the peak ground acceleration, estimated by Equation (4).

As an example, Figure 7 shows typical numerical predictions for the variation of $A_{Sa}^*$ in terms of the structure-to-soil fundamental period ratio ($T_{\text{str}}/T_S$) obtained for the same site, by applying two excitations with widely different frequency content but the same $a_{\max}^b$ ($=0.30g$). Observe that the frequency content of the excitation has a secondary effect on $A_{Sa}^*$. Furthermore, the numerical predictions follow some distinct trends, namely:

(a) for rigid structures ($T_{\text{str}} \cong 0$) the normalized spectral amplification ratio is $A_{Sa}^* \cong 1$,
(b) for structures with $T_{\text{str}} \cong T_S$ (resonance) the normalized spectral amplification ratio reaches a peak, hereafter denoted by $A_{Sa,p}^*$, and
(c) for more flexible structures ($T_{\text{str}}/T_s > 1$) the amplification ratio gradually decreases and tends asymptotically to a residual value, denoted by $A_{Sa,r}^*$.

These trends may be simulated by the following relatively simple analytical expression:

$$A_{Sa}^* = \frac{1 + B_1\left(\dfrac{T_{\text{str}}}{T_s}\right)^2}{\sqrt{\left(1 - \left(\dfrac{T_{\text{str}}}{T_s}\right)^2\right)^2 + \left(2B_2\dfrac{T_{\text{str}}}{T_s}\right)^2}} \tag{13}$$

 

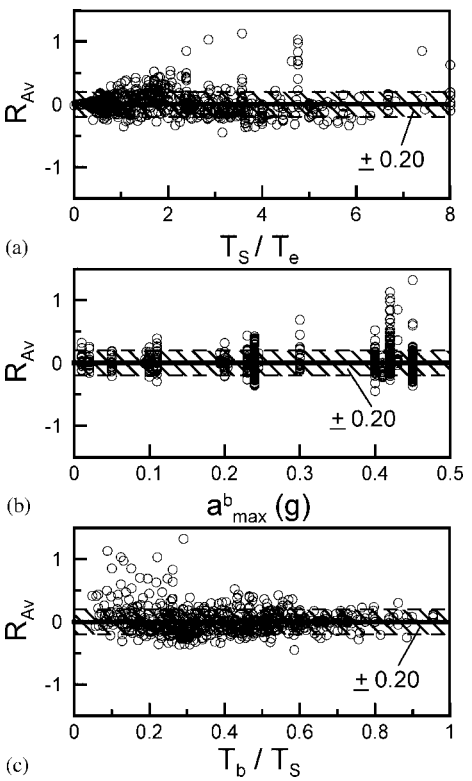


Figure 6. Evaluation of relative error in the computation of $A_V$ with the approximate relations (standard deviation of relative error = 0.20).

where parameters $B_1$ and $B_2$ can be expressed in terms of the peak $A^*_{Sa,p}$ and the residual $A^*_{Sa,r}$ values of $A^*_{Sa}$ according to:

$$B_1 = A^*_{Sa,r} \tag{14}$$

$$B_2 = \frac{1 + A^*_{Sa,r}}{2\,A^*_{Sa,p}} \tag{15}$$

This means that Equation (13) can be readily defined in terms of $A^*_{Sa,p}$ and $A^*_{Sa,r}$ alone. Hence, two independent statistical analyses were performed correlating $A^*_{Sa,p}$ and $A^*_{Sa,r}$ to the four known parameters $T_S/T_e$, $T_b/T_S$, $a^b_{\max}$ and $n$.

*Factors affecting* $A^*_{Sa,p}$

Figure 8 shows examples of the variation of $A^*_{Sa,p}$ as a function of the normalized soil period $T_S/T_e$, the most crucial of the four independent variables. Specifically, the data in this figure are presented in pairs of groups, by maintaining two of the other variables within a small range, and significantly changing the remaining independent variable.

 

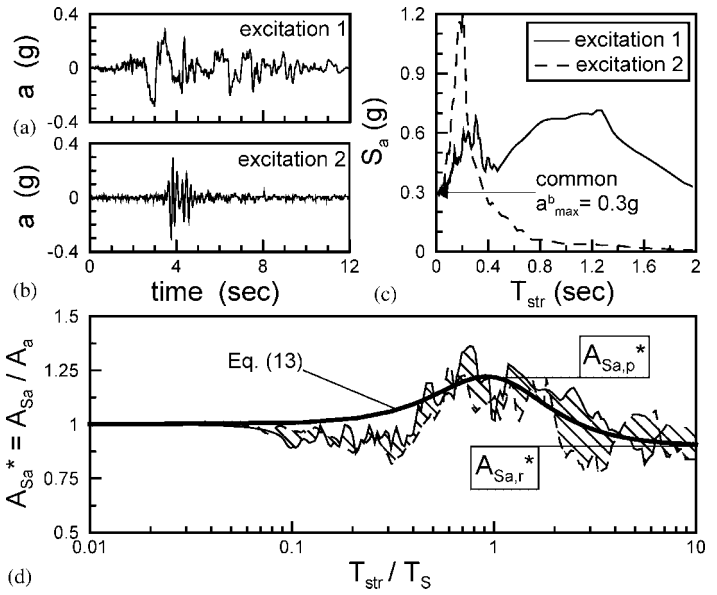


Figure 7. Typical ground-to-bedrock outcrop ratio of normalized elastic response spectra (5% damping) from equivalent-linear analyses: (a, b) acceleration time-histories of seismic excitations; (c) elastic response spectra of seismic excitations; (d) soil-to-bedrock outcrop ratio of normalized spectral accelerations.

In all cases, $A^*_{Sa,p}$ tends to 1.0 as $T_S/T_e$ tends to zero, it increases slightly for $0<T_S/T_e<1$ and then more rapidly for $T_S/T_e>1$. For relatively flexible profiles ($T_S/T_e>4$), the data points appear to stabilize around a more or less constant average value. Furthermore, these figures show that $A^*_{Sa,p}$ decreases with increasing $T_b/T_S$ and $n$, especially for $T_S/T_e>1$ (Figures 8(a) and (b)), but it is not significantly affected by the intensity of shaking (Figure 8(c)).

The above trends have been best-fitted by the following relation for $A^*_{Sa,p}$:

$$A^*_{Sa,p}=\begin{cases}1+c_{p1}\left(\dfrac{T_S}{T_e}\right)^{c_{p2}}, & \dfrac{T_S}{T_e}\leqslant 1\\[2ex] 1+c_{p1}+c_{p3}\left(\dfrac{T_b}{T_S}\right)^{c_{p4}} n^{c_{p5}}\left(\dfrac{T_S}{T_e}-1\right), & 1\leqslant\dfrac{T_S}{T_e}\leqslant 4\\[2ex] 1+c_{p1}+3c_{p3}\left(\dfrac{T_b}{T_S}\right)^{c_{p4}} n^{c_{p5}}, & 4\leqslant\dfrac{T_S}{T_e}\end{cases} \tag{16}$$

where: $c_{p1}=0.318$, $c_{p2}=0.058$, $c_{p3}=0.279$, $c_{p4}=-0.504$, $c_{p5}=-0.613$.

The constants in Equation (16) were determined using a stepped multi-variable regression analysis of the results of all numerical simulations. Specifically, the first analysis aimed at assessing whether the statistical insignificance of $a^b_{\max}$ that is shown in Figure 8(c) is corroborated by the actual data. Having established that $a^b_{\max}$ does not affect $A^*_{Sa,p}$ in a systematic manner, an analysis was consequently performed for merely the data that fall within the range of $1\leqslant T_S/T_e\leqslant 4$. This analysis provided the values of all constants in Equation (16), besides $c_{p2}$, which was estimated in the final analysis of merely the data that fall in the range of

 

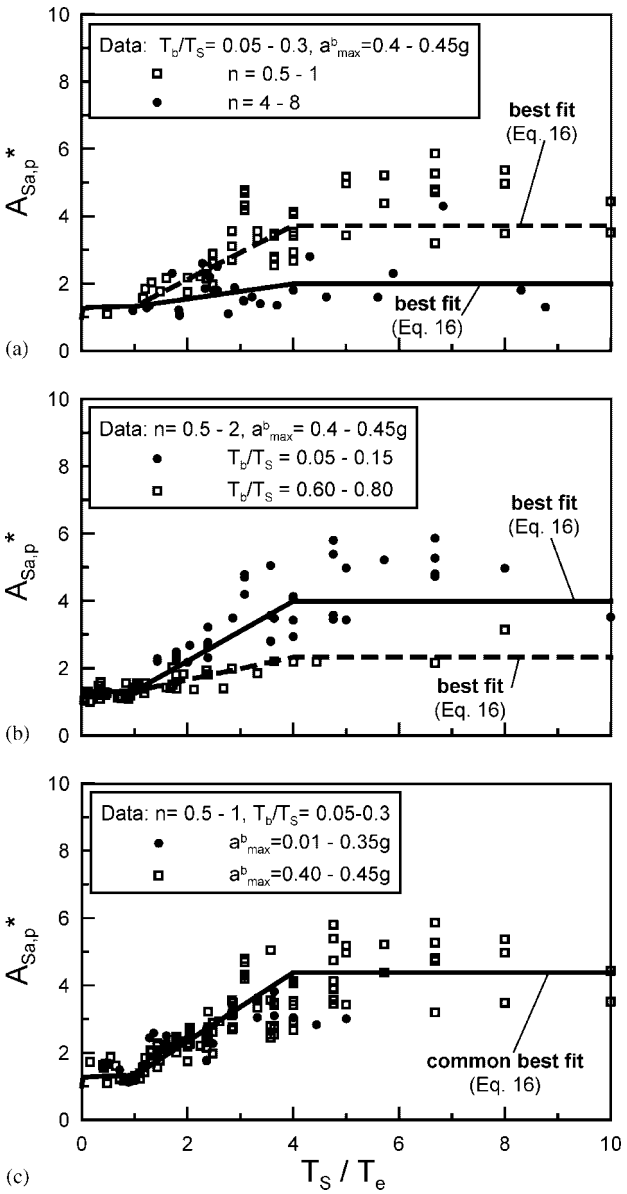


Figure 8. Effect of site and excitation parameters on $A^*_{Sa,p}$: (a) effect of equivalent number of cycles $n$; (b) effect of soil-to-bedrock impedance ratio $T_b/T_S$; (c) effect of peak bedrock acceleration $a^b_{\max}$.

$T_S/T_e \leqslant 1$. Obviously, by performing independent analyses for the three sets of data outlined by the ranges of $T_S/T_e$ in Equation (16), one could have obtained marginally more precise estimates. Nevertheless, such a methodology would not ensure the continuity of the proposed relations at $T_S/T_e = 1$ and 4.

 

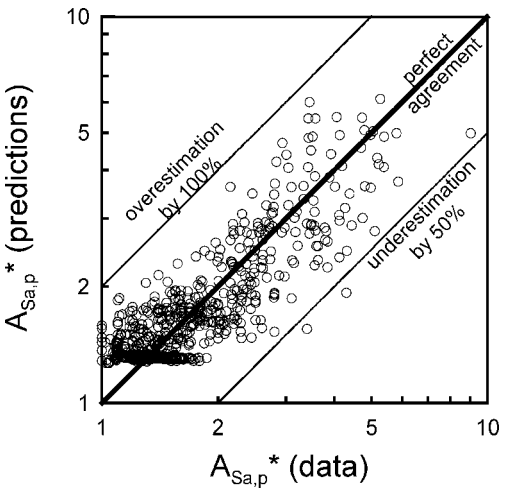


Figure 9. Summary comparison between predictions of $A^*_{Sa,p}$ from the approximate relations and their numerical estimates.

In order to quantify the accuracy of Equation (16), Figure 9 presents a one-to-one comparison of $A^*_{Sa,p}$ predictions to the corresponding data, while Figure 10 presents the relative error in $A^*_{Sa,p}$ predictions ($R_{A^*_{Sa,p}}$). Observe that, the $A^*_{Sa,p}$ values from Equation (16) agree well with their numerical simulations for all cases in the database. In detail, the relative error is more or less uniformly distributed over the entire range of the factors entering Equation (16), and has an overall standard deviation of 21%, without notable bias.

*Factors affecting* $A^*_{Sa,r}$

The general procedure in the analysis of the data for $A^*_{Sa,r}$ is the same as that followed for $A^*_{Sa,p}$. Hence, Figure 11 shows examples of the variation of $A^*_{Sa,r}$, primarily as a function of the normalized soil period $T_S/T_e$, and explores the effect of the remaining variables: $n$, $T_b/T_S$ and $a^b_{\max}$. In this case, $A^*_{Sa,r}$ tends to 1.0 as $T_S/T_e$ tends to zero, decreases slightly for $0<T_S/T_e<1$, but subsequently increases for $1<T_S/T_e$. For more flexible profiles ($T_S/T_e>6$), $A^*_{Sa,r}$ levels off and the data points become scattered around a constant average value. Furthermore, Figures 11(a) and (b) show that an increase in $T_b/T_S$ and $n$ results in a decrease in the value of $A^*_{Sa,r}$, especially for $T_S/T_e>1$, while Figure 11(c) shows that the intensity of the shaking does not affect significantly the value of $A^*_{Sa,r}$.

The following relation expresses these trends, in analytical form:

$$A^*_{Sa,r}=\begin{cases} 1+c_{r1}\left(\dfrac{T_s}{T_e}\right), & \dfrac{T_S}{T_e}\leqslant 1 \\ 1+c_{r1}+c_{r3}\left(\dfrac{T_b}{T_s}\right)^{c_{r4}} n^{c_{r5}}\left(\dfrac{T_s}{T_e}-1\right), & 1\leqslant\dfrac{T_S}{T_e}\leqslant 6 \\ 1+c_{r1}+5c_{r3}\left(\dfrac{T_b}{T_s}\right)^{c_{r4}} n^{c_{r5}}, & 6\leqslant\dfrac{T_S}{T_e} \end{cases} \tag{17}$$

 

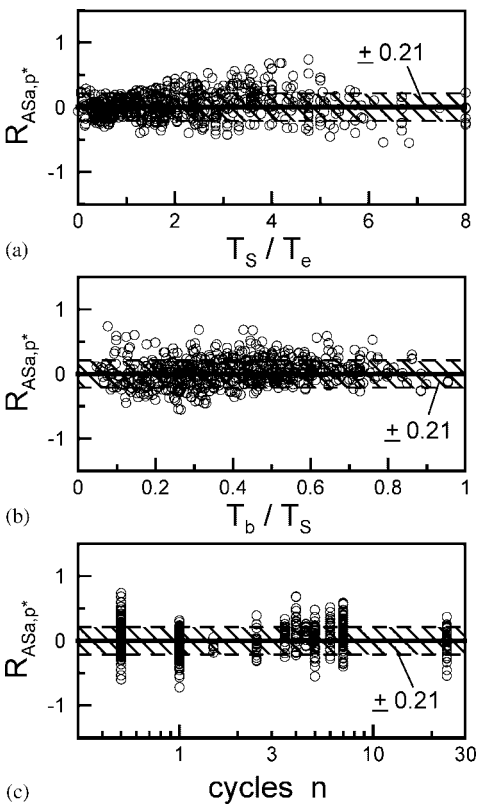


Figure 10. Evaluation of relative error in the computation of $A^*_{Sa,p}$ with the approximate relations (standard deviation of relative error = 0.21).

Using essentially the same steps as for $A^*_{Sa,p}$, the constants in Equation (17) were determined as: $c_{r1} = -0.302$, $c_{r3} = 0.189$, $c_{r4} = -0.474$, $c_{r5} = -0.406$.

The accuracy of the proposed relation for $A^*_{Sa,r}$ is evaluated in Figures 12 and 13, in the same format as for $A^*_{Sa,p}$. The agreement between approximate and numerical predictions is fairly systematic. Namely, the overall relative error has a standard deviation of about 26%, without significant bias with respect to the factors entering Equation (17).

## RELATION FOR SOIL PERIOD

In order to apply the previous relations in practice, one has to provide the peak acceleration at the outcropping bedrock $a^b_{\max}$, the predominant period of the excitation $T_e$, as well as the fundamental vibration periods for the bedrock $T_b$ and for the soil $T_S$. Among these parameters, $a^b_{\max}$ and $T_e$ are usually provided by a seismic hazard study, while $T_b$ is related by definition to the soil thickness $H$ and the elastic shear wave velocity of the bedrock $V_b$ (i.e. $T_b = 4H/V_b$, by assuming linearity for the bedrock). However, estimation of $T_S$ is not equally straightforward, even if the variation of elastic shear wave velocity with depth is known. This is mostly due

 

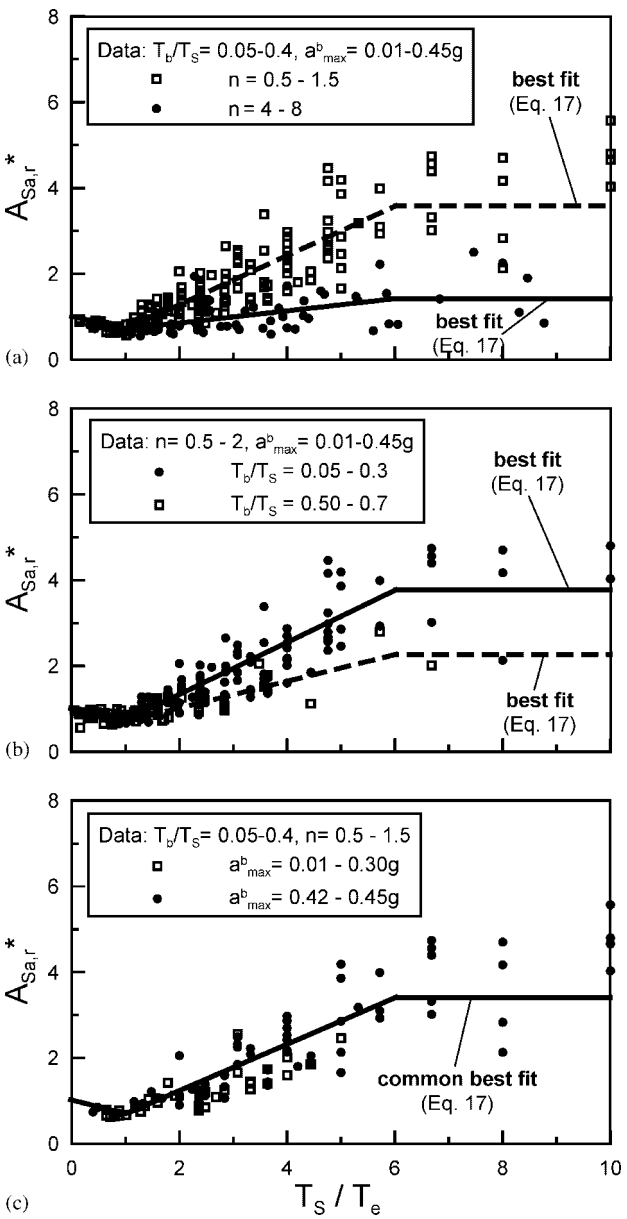


Figure 11. Effect of site and excitation parameters on $A^*_{Sa,r}$: (a) effect of equivalent number of cycles $n$; (b) effect of soil-to-bedrock impedance ratio $T_b/T_S$; (c) effect of peak bedrock acceleration $a^b_{\max}$.

 

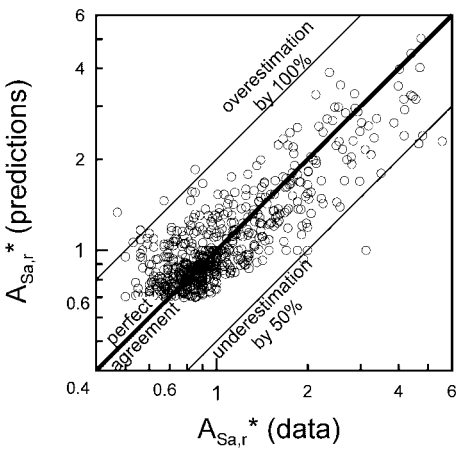


Figure 12. Summary comparison between predictions of $A^*_{Sa,r}$ from the approximate relations and their numerical estimates.

to the fact that soil response during shaking is non-linear and consequently the fundamental vibration non-linear period $T_S$ is related to the applied shear stresses and strains in addition to the elastic soil properties.

Soil non-linearity can be depicted by many methods, but for the purpose of our study what is most important is how the elastic shear modulus $G_o$ degrades to each ever-current secant value $G$ as a function of the applied cyclic shear strain amplitude $\gamma$. It can be shown that experimental curves of shear modulus degradation with shear strain (e.g. those of Vucetic and Dobry [15]) can be approximately expressed as:

$$\frac{G}{G_o} = \frac{1}{1 + \kappa\gamma^{\lambda}} \tag{18}$$

where $\kappa$ and $\lambda$ are positive constants. In terms of shear wave velocities, Equation (18) becomes:

$$\left(\frac{V_S}{V_{S,o}}\right)^2 = \frac{1}{1 + \kappa\gamma^{\lambda}} \tag{19}$$

where $V_S$ denotes the shear wave velocity for cyclic shear strain amplitude $\gamma$ and $V_{S,o}$ denotes the linear (elastic) shear wave velocity corresponding to $\gamma < 10^{-5}$.

Based on Equation (19), and in view of the fact that the period of uniform soil profiles is inversely proportional to the shear wave velocity, a general relation for the fundamental soil period $T_S$ is:

$$\left(\frac{T_S}{T_{S,o}}\right)^2 = 1 + \kappa\gamma^{\lambda} \tag{20}$$

where $T_{S,o}$ denotes the linear (elastic) soil period (for $\gamma < 10^{-5}$).

 

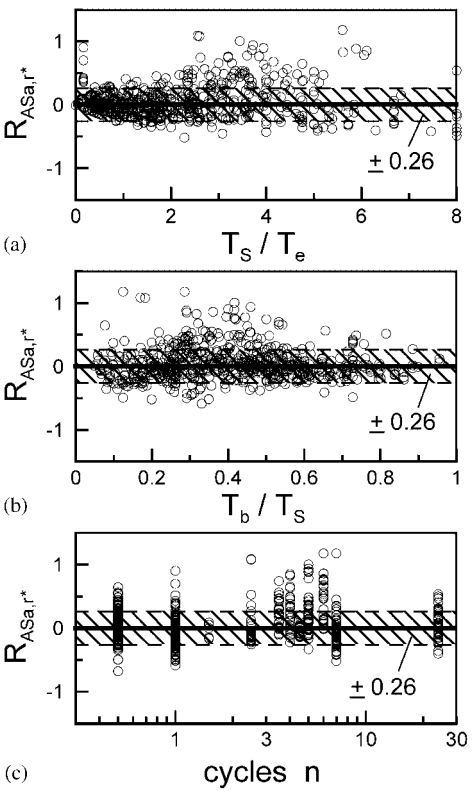


Figure 13. Evaluation of relative error in the computation of $A^*_{Sa,r}$ with the approximate relations (standard deviation of relative error = 0.26).

On a layer level, the cyclic shear strain amplitude $\gamma$ is a function of the secant soil stiffness $G$, but also the earthquake-induced cyclic shear stress $\tau$. Similarly, on a site level, $\gamma$ in Equation (20) may be related to two macroscopic, and directly measurable, parameters: (a) the average elastic shear wave velocity of the soil $\bar{V}_{S,o}$, as an index of the average $G$ value for the site, and (b) the peak acceleration at outcropping bedrock $a^b_{\max}$, as an index of the average applied $\tau$ for the site. Hence:

$$\left(\frac{T_s}{T_{s,o}}\right)^2 = 1 + d_{1,T}(\bar{V}_{s,o})^{d_{2,T}}\left(\frac{a^b_{\max}}{g}\right)^{d_{3,T}} \tag{21}$$

with $d_{1,T}$ and $d_{3,T} > 0$, while $d_{2,T} < 0$. The values of these constants were estimated from a multivariable regression analysis of all available data, as: $d_{1,T} = 5330$, $d_{2,T} = -1.30$ and $d_{3,T} = 1.04$.

Figure 14 presents a one-to-one comparison between $T_S$ predictions and results from the equivalent-linear analyses (data). In addition, Figure 15 correlates the relative error $R_{T_S}$ to the two basic input parameters $a^b_{\max}$ and $\bar{V}_{S,o}$. It can be argued that the proposed relation follows closely the basic trends of the data, in qualitative as well as in quantitative terms. The standard deviation of the relative error is 24% on average, but increases with $a^b_{\max}$. This

 

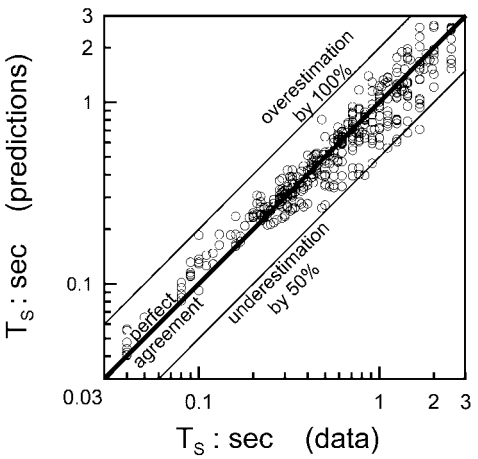


Figure 14. Summary comparison between predictions for $T_S$ from the approximate relations and their numerical estimates.

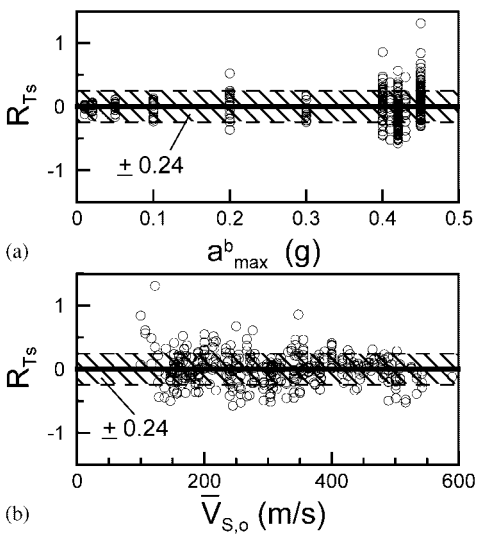


Figure 15. Evaluation of relative error in the computation of $T_S$ with the approximate relations (standard deviation of relative error = 0.24).

non-uniformity of the error is natural, since soil response becomes practically elastic as $a^b_{\max}$ tends to zero, and consequently $R_{T_s}$ tends by definition to zero.

## VERIFICATION CASE STUDIES

In this section the proposed multi-variable relations are applied in seven well-documented actual case studies of soil amplification: (a) two sites in the San Fernando Valley during

 

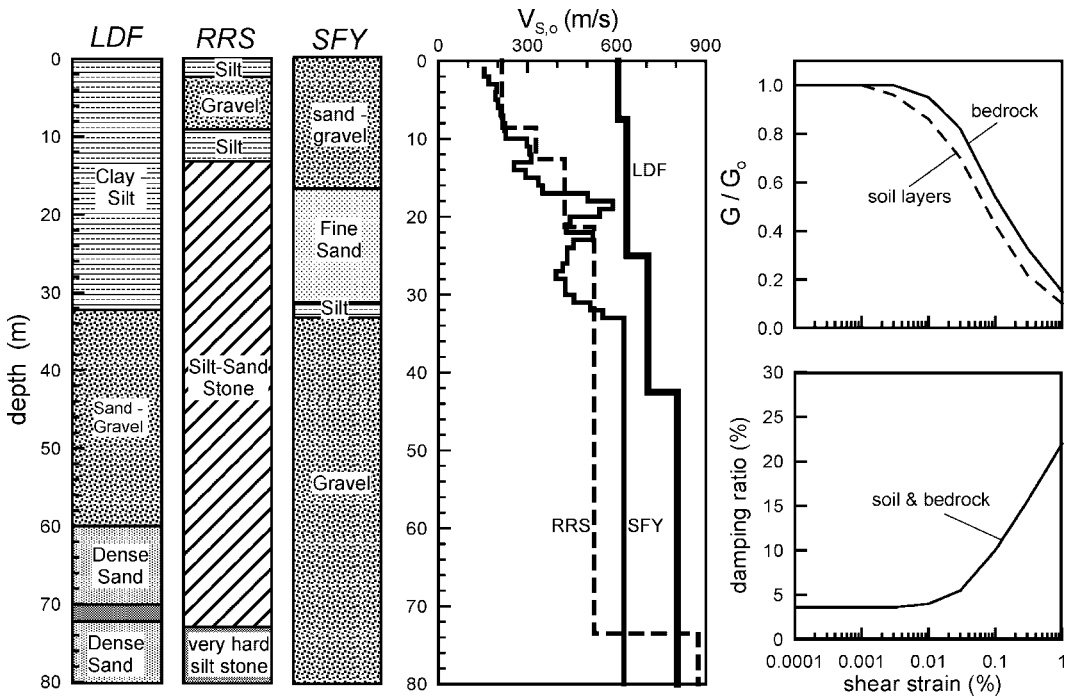


Figure 16. Geological and geotechnical information for LDF, RRS and SFY sites [25].

the Northridge earthquake (17 January 1994), and (b) five seismic events recorded by the SMART-1 accelerometer array in Taiwan. The main goal of this application is to ascertain the reliability and the robustness of the proposed relations and also to guide their application in practice. For the benefit of brevity, the geological, geotechnical and seismological data pertaining to the seven case studies are simply outlined, but properly referenced, below.

### *Northridge earthquake*

The Northridge earthquake ($M_w = 6.7$) has been recorded at the surface of three nearby sites within the San Fernando Valley: Los Angeles Dam (LDF), Rinaldi Receiving Station (RRS) and Arleta Fire Station (SFY). The geological profile and the measured $V_{S,o}$ variation with depth at the three sites are shown in Figure 16. Observe that while the RRS and SFY sites are relatively soft near the surface ($V_{S,o} \leqslant 400$ m/s for the top 16 m), site LDF is consistently stiffer ($V_{S,o} > 600$ m/s for all depths). In view of these geotechnical properties, the close distance between the sites (less than 4 miles) and the proximity between their respective epicentral distances (approximately 8–10 miles), LDF is considered as the bedrock outcrop site and RRS and SFY as its associated soil sites. For further details on the geological, geotechnical and seismological data, see Cultrera *et al.* [25].

 

Table II. Site and excitation parameters for the seven verification case studies.

| Case | $a^b_{\max}$ ($g$) | $V^b_{\max}$ (m/s) | $T_e$ (s) | $n$ | $H$ (m) | $\bar{V}_{S,o}$ (m/s) | $T_b$ (s) | $T_{S,o}$ (s) | $T_S$ (s) |
|---|---|---|---|---|---|---|---|---|---|
| RRS | 0.291 | 0.756 | 1.00 | 4 | 73.5 | 494 | 0.37 | 0.59 | 0.72 |
| SFY | 0.291 | 0.756 | 1.00 | 4 | 33.5 | 408 | 0.21 | 0.33 | 0.42 |
| 29 | 0.033 | 0.032 | 0.22 | 5 | 80.0 | 283 | 0.58 | 1.13 | 1.19 |
| 39 | 0.200 | 0.131 | 0.16 | 2 | 80.0 | 283 | 0.58 | 1.13 | 1.45 |
| 40 | 0.190 | 0.199 | 0.20 | 1.5 | 80.0 | 283 | 0.58 | 1.13 | 1.44 |
| 41 | 0.050 | 0.023 | 0.19 | 3 | 80.0 | 283 | 0.58 | 1.13 | 1.22 |
| 45 | 0.140 | 0.240 | 0.20 | 2.5 | 80.0 | 283 | 0.58 | 1.13 | 1.36 |

For applying the proposed relations for the sites in question, the seismic excitation (recording at LDF) is quantified in terms of $a^b_{\max}$, $n$ and $T_e$, based on its NS component that provided the strongest acceleration and velocity [25]. Then, to compute $T_{s,o}$, appropriate depths $H$ to bedrock are assumed for the RRS and SFY sites, respectively, and the simplified version of the Rayleigh procedure [23] is used in connection with the measured $V_{S,o}$ profile. An outline of the values of $a^b_{\max}$, $T_e$, $n$, $H$, average $\bar{V}_{S,o}$, $T_b$, $T_{S,o}$ and $T_S$ for RRS and SFY during the Northridge earthquake is presented in Table II.

Overall, soil amplification at these two sites is estimated by three methods: (a) direct calculation from the actual *recorded* time-histories in the surface of nearby 'soil' and 'bedrock' sites, (b) *approximate* calculations via the proposed relations, and (c) *numerical* calculations with the equivalent-linear method (using SHAKE91). The latter were performed with the site parameters presented in Figure 16, where the denoted $G/G_o$ and damping curves are averages from measurements [25]. Obviously, the numerical results are affected by the assumed average $G/G_o$ and damping curves, but a sensitivity analysis is beyond the scope of this paper. Rather, two analyses were performed for each site, by successively setting each horizontal component of the recorded motion at LDF as the seismic excitation at the corresponding bedrock outcrop.

The elastic response spectra from the three methods for sites RRS and SFY are compared in Figures 17 and 18, respectively. Specifically, Figures 17(a) and 18(a) compare the approximately predicted to the recorded elastic response spectra. Each of Figures 17(a) and 18(a) consist of three plots: the upper plot that compares the normalized amplification response spectra, $A^*_{Sa}$; the intermediate that compares the response spectra at the soil surface, $S^s_a$; and the lower plot that provides a direct estimate of the error in the prediction of $S^s_a$, in terms of the ratio of predicted-over-recorded values. The results of the aforementioned equivalent-linear analyses for the RRS and SFY soil sites are compared with the records in Figures 17(b) and 18(b), respectively, by using the same three-partite plotting scheme. Finally, Figures 17(c) and 18(c) compare the foregoing numerical results to predictions obtained with the proposed multi-variable relations.

The proposed relations underpredict $S^s_a$ for the RRS site (Figure 17(a)), by practically the same amount for all structural periods $T_{\text{str}}$, and slightly over-predict the recorded values for the SFY site (Figure 18(a)). However, Figures 17(b) and 18(b) show that the numerical analyses offer similar predictions with respect to the records. It also suggests that the statistical

 

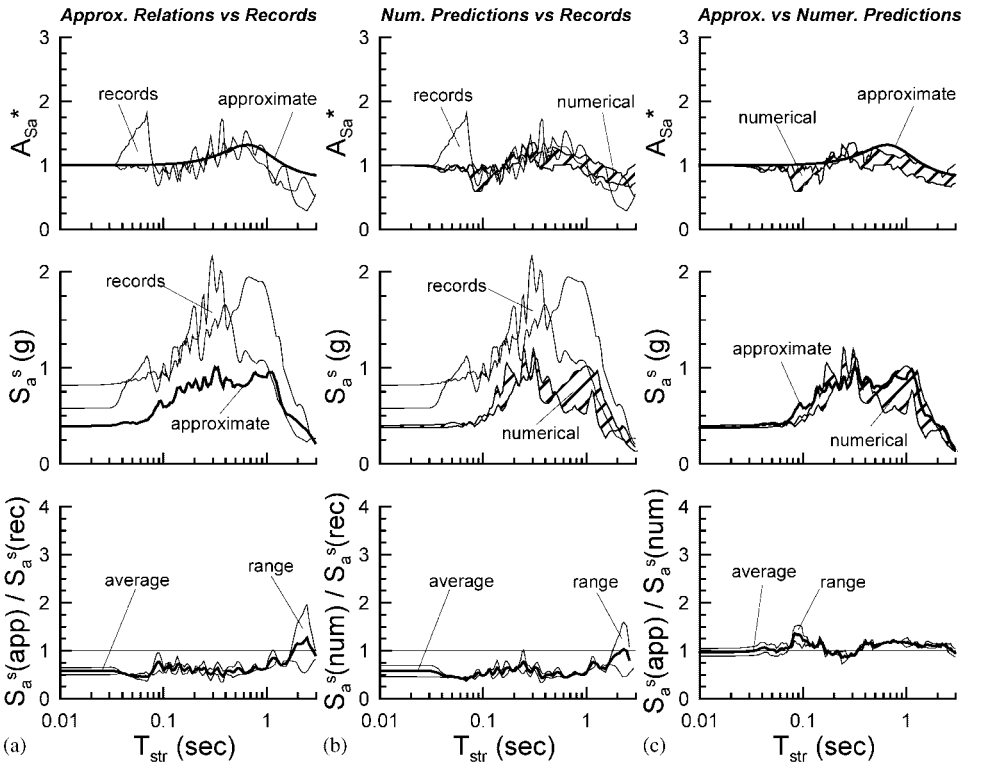


Figure 17. Evaluation of approximate relations for the elastic response spectra for the RRS site during the Northridge event: (a) approximate relations vs recordings; (b) numerical predictions vs recordings; (c) approximate relations vs. numerical predictions.

accuracy of the approximate predictions is comparable to that of the numerical predictions. This is better depicted in Figures 17(c) and 18(c), where the predictions from the proposed relations are directly compared to the numerical results. Observe that, for the most part, the former are within $\pm 30\%$ of the latter.

### *SMART-1 accelerometer array*

The SMART-1 array is located on a flat plain in a basin of triangular shape that is 15 km wide and 8 km long [26]. The geological materials of the plain consist of recent soil and alluvium layers (thickness 30–80 m) at the surface and a stiffer Pleistocene layer (thickness 170–540 m) that overlies the Miocene rock basement [27]. The subsurface layers can be assumed as practically horizontal.

Of special interest to this study are two stations: (a) soil site O-07 at the south side of the array and (b) bedrock outcrop site E-02 that is installed at approximately 2.8 km to the south of O-07, where the Miocene bedrock formation appears on the surface. Figure 19 presents the

 

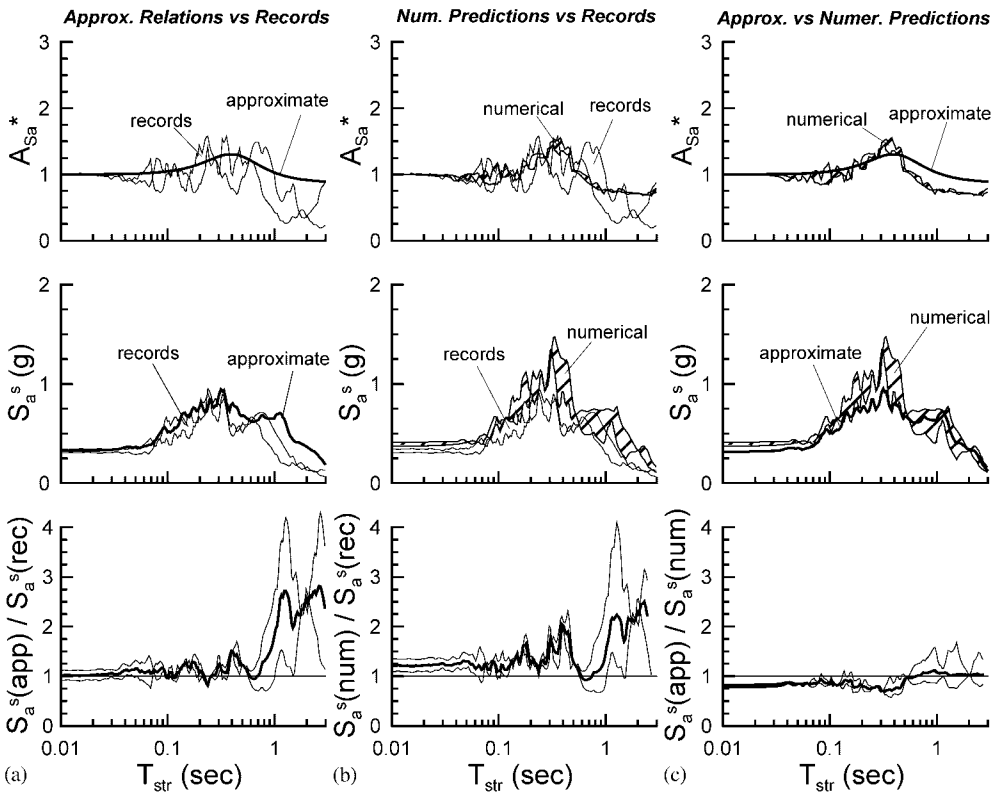


Figure 18. Evaluation of approximate relations for the elastic response spectra for the SFY site during the Northridge event: (a) approximate relations vs recordings; (b) numerical predictions vs recordings, and (c) approximate relations vs numerical predictions.

$V_{S,o}$ profile with depth at the O-07 soil site [28]. Observe that it is a soft soil site, with $V_{S,o}$ as low as 120 m/s near the surface and greater than 400 m/s at a depth of 80 m. The apparent contrast in $V_{S,o}$ at a depth of 80 m dictated the assumption of $H = 80$ m for this site, despite the fact that it is not clear whether this contrast corresponds to an interface with Pleistocene or older materials. According to the simplified version of the Rayleigh procedure [23] and the $V_{S,o}$ profile of Figure 19, the fundamental linear soil period for this depth to bedrock is $T_{S,o} = 1.13$ s. The respective value for the bedrock is $T_b = 0.58$ s.

Numerous earthquakes have been recorded at both the O-07 and the E-02 sites over the years. In this paper, five events are used with epicentral distances $R = 22$–79km and $M_L = 6$–7. The values of $a_{\max}^b$, $T_e$, $n$, $H$, average $\bar{V}_{S,o}$, $T_b$, $T_{S,o}$ and $T_S$ for site O-07 during the five seismic events are presented in Table II. Observe that owing to soil non-linearity, the difference between $T_S$ and $T_{S,o}$ is larger for the stronger events 39, 40 and 45 than for the weaker ones 29 and 41.

As in the case of the Northridge earthquake, soil amplification was estimated by means of the proposed relations, the records, as well as numerical analyses with SHAKE91

 

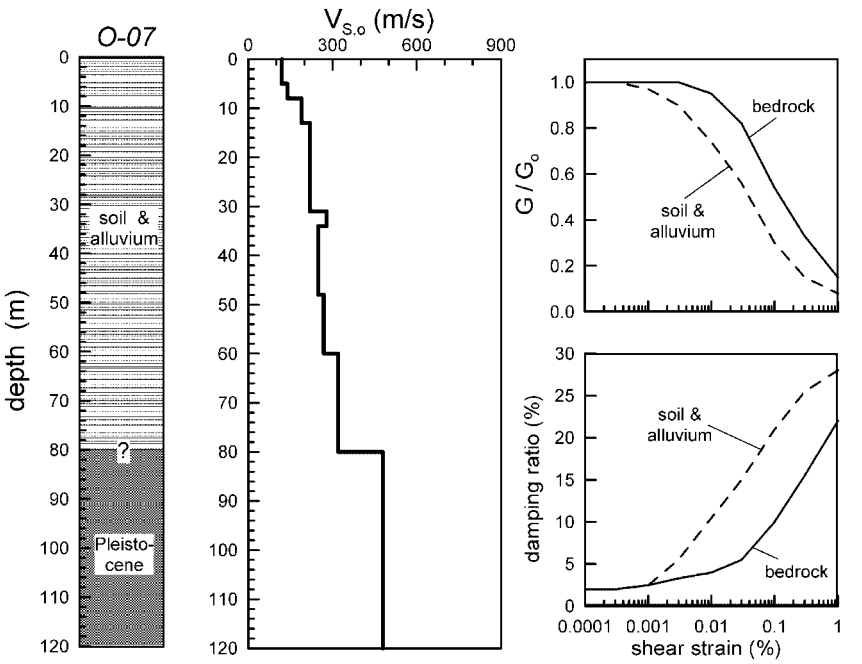


Figure 19. Geological and geotechnical information for soil site O-07 in the SMART-1 seismic array [18, 28].

for all five events. Nevertheless, for reasons of brevity, comparisons between approximate, recorded and numerically predicted elastic response spectra are shown only for seismic events 29 and 45, i.e. a low intensity and a high intensity event, in Figures 20 and 21, respectively. Observe in Figures 20(a) and 21(a) that the proposed methodology provides a reasonably satisfactory prediction of the recorded amplification. It is also interesting to note that the results obtained from the numerical analyses (Figures 20(b) and 21(b)) are of similar accuracy. This becomes more evident in Figures 20(c) and 21(c), where the numerical results are compared directly to the predictions from the multivariable relations.

In Figures 17, 18, 20 and 21 comparisons are made for the elastic response spectra. Hence, the accuracy in the prediction of $A_a$ can be assessed only indirectly. In addition, no evidence is given for the accuracy in the prediction of $A_V$. These deficiencies are remedied in Figure 22, where the associated $A_a$ and $A_V$ values for all seven case studies are presented. Overall, there are two points to be observed in this figure. The first is that the approximate predictions are in fair and consistent agreement with the numerical results ($\pm 45\%$ in Figures 22(c) and (f)). The second point is that both approximate and numerical predictions are in only broad agreement with the recordings. The observed scatter is a reminder of the widely acknowledged difficulties encountered when field data are interpreted on the basis of theoretical models (the equivalent-linear method and the proposed relations in this paper).

 

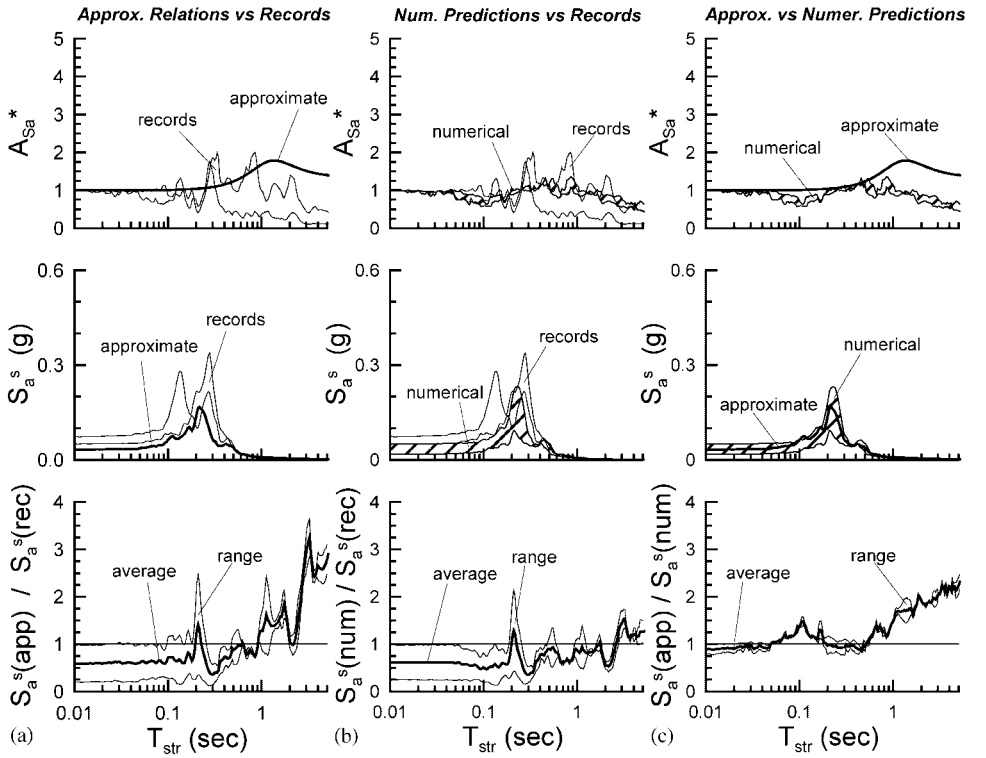


Figure 20. Evaluation of approximate relations for the elastic response spectra for site O-07 during Event 29; (a) approximate relations vs recordings; (b) numerical predictions vs recordings; (c) approximate relations vs numerical predictions.

## CONCLUSIONS

A set of approximate, multivariable relations is established to evaluate soil effects on the peak horizontal acceleration, the peak horizontal velocity and the horizontal elastic response spectra (5% damping). The basic innovation of the approach is the use of results from numerical analyses of seismic ground response instead of seismic recordings. The overall validity of the approach is verified against seven well-documented case studies of soil amplification from the San Fernando Valley during the Northridge earthquake and various events at the SMART-1 array in Taiwan.

Based on the results of the statistical analysis and the verification of the proposed relations presented herein, the following conclusions are made.

(a) Soil effects on peak ground acceleration can be expressed as a function of the normalized soil period ($T_S/T_e$), the peak acceleration at the outcropping bedrock ($a^b_{\max}$), the bedrock-to-soil fundamental period ratio ($T_b/T_S$), and the duration of the seismic excitation, expressed via the number of equivalent cycles of harmonic excitation ($n$). Soil effects on peak ground velocity depend on the same parameters, except for $n$.

 

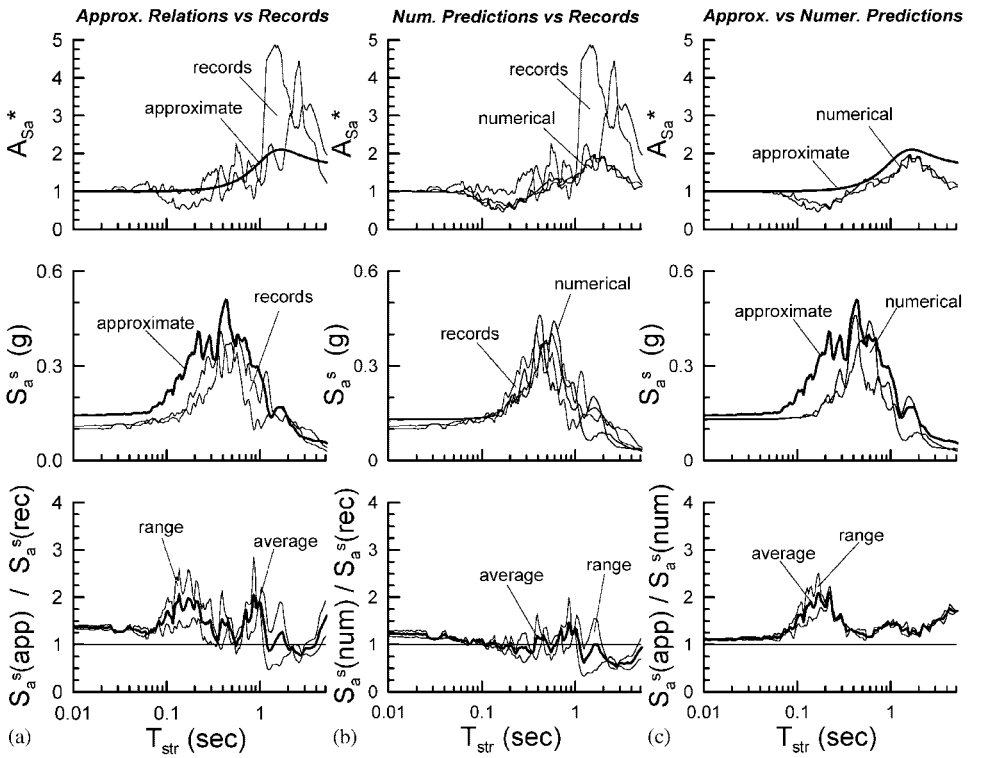


Figure 21. Evaluation of proposed relations for the elastic response spectra for site O-07 during Event 45: (a) approximate relations vs recordings; (b) numerical predictions vs recordings; (c) approximate relations vs numerical predictions.

(b) Soil effects on the normalized elastic response spectra are primarily a function of the normalized periods $T_{\mathrm{str}}/T_S$ and $T_S/T_e$ and secondarily of the bedrock-to-soil fundamental period ratio $T_b/T_S$ and the number of cycles $n$. The peak acceleration of the seismic excitation $a_{\max}^b$ is statistically insignificant.

(c) In addition, the non-linear soil period $T_S$ is related to the linear soil period $T_{S,o}$, the average elastic shear wave velocity $\bar{V}_{S,o}$ over the entire soil depth, and $a_{\max}^b$.

(d) *Best-fit* predictions obtained from the proposed relations compare well with the respective estimates from equivalent-linear analyses. No distinct bias is observed and the overall standard deviation of the relative error in the estimation of the studied measures of soil amplification varies between 20% and 26%.

(e) Based on the verification case studies it can be argued that similar accuracy levels are obtained when either the proposed relations or the equivalent linear method are used to predict the soil amplification from actual seismic recordings.

Note that the range of the site and excitation parameters listed in Table I essentially defines the limits of application of the proposed relations. Furthermore, it should be acknowledged

 

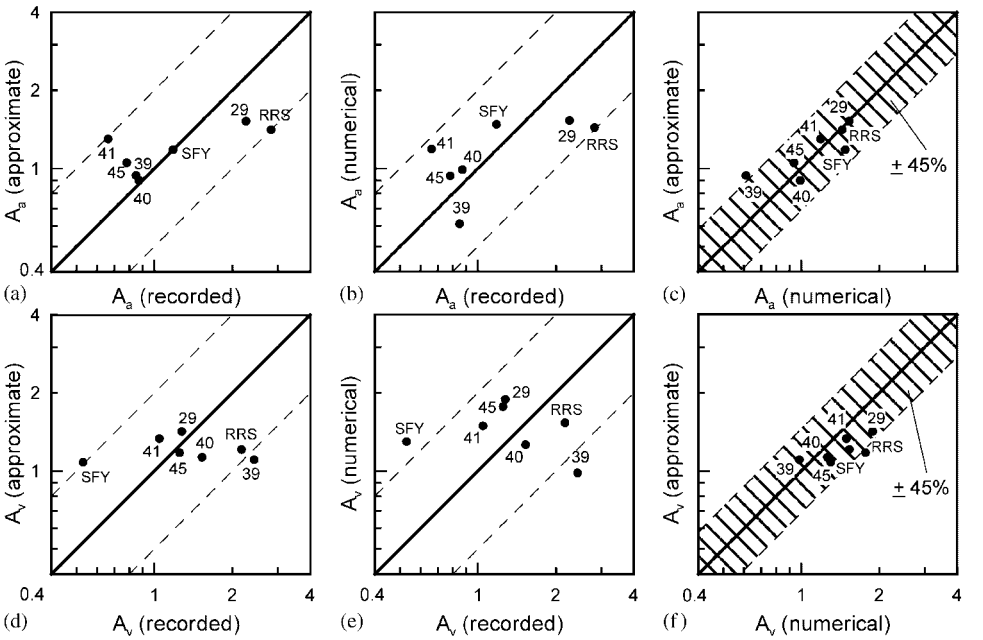


Figure 22. Evaluation of proposed *best fit* relations against seismic recordings and numerical predictions: (a), (b), (c) evaluation of $A_a$; (d), (e), (f) evaluation of $A_V$.

that the conclusions, as well as all relations proposed for the evaluation of soil effects, draw upon the equivalent linear method of analysis and consequently inherit both its advantages, as well as its shortcomings. Thus, the approximate relations should be viewed as a user-friendly, robust alternative to the equivalent linear method and should be used with the same reservations.

## ACKNOWLEDGEMENTS

This research was funded by the Earthquake Protection and Planning Organization of Greece (Ο.Α.Σ.Π). Professor George Gazetas of the National Technical University of Athens has contributed valuable comments on the presentation of the paper. Dr Nickolaos Theodulidis, Director of the Institute of Engineering Seismology and Earthquake Engineering in Thessaloniki (Ι.Τ.Σ.Α.Κ.), provided the seismological data pertaining to the SMART-1 accelerometer array. Finally, fellow Civil Engineers Thomas Panourgias and Michael Klouvas assisted with the statistical analysis and Niki Kringos (Civil Engineer, TU Delft) assisted with the verification of the relations. All these contributions are gratefully acknowledged.

## REFERENCES

1. Ambraseys NN, Simpson KA, Bommer JJ. Prediction of horizontal response spectra in Europe. *Earthquake Engineering and Structural Dynamics* 1996; **25**:371–400.
2. Boore DM, Joyner WD, Fumal TE. Estimation of response spectra and peak accelerations from Western North America earthquakes: An interim report. *U.S.G.S.*, *Open File Report 93-509*; 1993; p. 72.

 

3. Boore DM, Joyner WD, Fumal TE. Estimation of response spectra and peak accelerations from Western North America earthquakes: An interim report (Part 2). *U.S.G.S.*, *Open File Report 94-127*; 1994; p. 40.
4. Boore DM, Joyner WD, Fumal TE. Empirical near-source attenuation relationships for horizontal and vertical peak ground acceleration, peak ground velocity and pseudo-absolute acceleration response spectra. *Seismological Research Letters* 1997; **168**(1):154–179.
5. Borcherdt RD. Estimates for site dependent response spectra for design (methodology and justification). *Earthquake Spectra* 1991; **10**(4):617–653.
6. Kawashima K, Aizawa K, Takashi K. Attenuation of peak ground acceleration, velocity and displacement based on multiple regression analysis of Japanese strong ground motion records. *Earthquake Engineering and Structural Dynamics* 1986; **14**:199–218.
7. Midorikawa S, Matsuoka M, Sakugawa K. Site effects on strong motion records observed during the 1987 Chiba-ken-toho-oki, Japan earthquake. *Proceedings of the 9th Japan Earthquake Engineering Symposium*, vol. 3: 85–90, Tokyo, December, 1994.
8. Spudich P, Joyner WB, Lindh AG, Boore DM, Margaris BM, Fletcher JB. SEA99 – A revised ground motion prediction relation for use in extensional tectonic regimes. *Bulletin of the Seismological Society of America* 1999; **89**(5):1156–1170.
9. Schnabel PB, Lysmer J, Seed HB. SHAKE – A computer program for earthquake response analyses of layered soils. *Research Report EERC — 72* 1972; Berkeley, CA.
10. Idriss IM, Sun JI. SHAKE91 – A computer program for conducting equivalent linear seismic response analysis of horizontally layered soil deposits. *User*'s *Guide*, Center for Geotechnical Modeling, Civil Engineering Department, U.C. Davis, 1992.
11. Lee M, Finn L. Program for the dynamic effective stress response analysis of soil deposits including liquefaction evaluation. *Research Report*, *University of British Columbia*, *Faculty of Applied Sciences*; 1978.
12. Mellal A, Modaressi H. A simplified numerical approach for nonlinear dynamic analysis of multi-layered media. *Proceedings of the 11th European Conference on Earthquake Engineering*, Paris, 6–11 September 1998.
13. Bouckovalas GD. Prediction of soil effects on seismic motions: A comparative case study. *Earthquake Spectra* 1997; **13**(3):333–361.
14. Kramer SL. *Geotechnical Earthquake Engineering*. Prentice Hall; 1996; p. 653.
15. Vucetic M, Dobry R. Effect of soil plasticity on cyclic response. *Journal of Geotechnical Engineering* (ASCE) 1991; **117**(1):89–107.
16. Borja RI, Chao HY, Montans FJ, Lin CH. Non-linear ground response at Lotung LSST site. *Journal of Geotechnical and Geoenvironmental Engineering* (ASCE) 1999; **125**(3):187–197.
17. Chang C-Y, Mok CM, Power MS. Analysis of ground response data from Lotung large-scale soil-structure interaction experiment site. *Report NP-7306-SL*, *Electric Power Research Institute* 1991; Palo Alto, California.
18. Chang C-Y, Mok CM, Tang H-T. Inference of dynamic shear modulus from Lotung downhole data. *Journal of Geotechnical Engineering* (ASCE) 1996; **122**(8):657–665.
19. Mok CM, Chang C-Y, Legaspi DE. Site response analyses of vertical excitation. *Proceedings of Geotechnical Earthquake Engineering and Soil Dynamics III*, *ASCE*, Seattle, Washington, 3–6 August 1998.
20. Soeda Y, Tamai H, Nakatsu N. Nonlinearity and irregularity of strong seismic motions by vertical arrays during the 1995 Kobe earthquake. *Proceedings of the 2nd International Conference on Earthquake Geotechnical Engineering*, Lisbon, pp. 225–230, 21–25 June 1999.
21. Kausel E, Assimaki D. Seismic simulation of inelastic soils via frequency-dependent moduli and damping. *Journal of Engineering Mechanics* (ASCE) 2002; **128**(1):34–47.
22. Yoshida N, Kobayashi S, Suetomi I, Miura K. Equivalent linear method considering frequency dependent characteristics of stiffness and damping. *Soil Dynamics and Earthquake Engineering* 2002; **22**:205–222.
23. Biggs JM. *Introduction to Structural Dynamics*. McGraw-Hill; 1965; p. 341.
24. Chopra AK. *Dynamics of Structures: Theory and Applications to Earthquake Engineering*. Prentice Hall, 1995; p. 729.
25. Cultrera G, Boore DM, Joyner WB, Dietel CM. Nonlinear soil response in the vicinity of the Van Norman Complex following the 1994 Northridge California, earthquake. *Bulletin of the Seismological Society of America* 1999; **89**(5):1214–1231.
26. Elgamal A-W, Zeghal M, Parra E, Gunturi R, Tang HT, Stepp JC. Identification and modeling of earthquake ground response – I. Site amplification. *Soil Dynamics and Earthquake Engineering* 1996; **15**(8):499–522.
27. Wen KL, Yeh YT. Seismic velocity structure beneath the SMART1 array. *Bulletin of the Institute of Earth Sciences* 1984; **4**:51–72.
28. Wen KL. Non-linear soil response in ground motions. *Earthquake Engineering and Structural Dynamics* 1994; **23**:599–608.

 